SCIENTIFIC JOURNAL
EARTH'S CRYOSPHERE

Earth`s Cryosphere, 2014, vol. XVIII, No. 3, pp. 76–82 http://earthcryosphere.ru/

SAFETY OF FOUNDATIONS AND STRUCTURES IN PERMAFROST

BUILDING ON PERMAFROST: ENGINEERING SOLUTIONS FOR ENERGY EFFICIENCY

V.P. Melnikov, A.A. Melnikova*, G.V. Anikin*, K.S. Ivanov*, K.A. Spasennikova*

Tyumen State Oil and Gas University, 38 Volodarskogo str., Tyumen, 625000, Russia
** Institute of Earth's Cryosphere, Siberian Branch of the Russian Academy of Sciences, 86 Malygina str., Tyumen, 625000, Russia; anikin@ikz.ru*

Stochastic analysis has been applied to predict the thermal behavior of soil under a structure built on permafrost without piles. The obtained models simulate different possible scenarios at three options of thermal insulation between the building and the soil, with diatomite-based foam glass and penoplex insulation materials and with thermosyphon natural cooling systems. If a building lacks a ventilated cellar, the soil under it will thaw sooner or later without thermosyphons. High energy efficiency can be achieved by using insulation materials with low thermal conductivity, such as diatomite-based foam glass, along with thermosyphon cooling.

Seasonal cooling system, thermosyphon, soil, foundation, basement, diatomite foam glass, penoplex

INTRODUCTION

Development of the Arctic natural resources requires ever more construction on permafrost, with increasing demand for methods of soil stabilization beneath civil and engineering structures. The pile foundation issues have been quite well studied while construction without piles requires further investigation and numerical tests. In this paper, we model the thermal effect of a building, with the indoor temperature 20 °C, at three options of protecting the soil from heating: two thermal insulation materials of foamed glass based on diatomaceous earth or diatomite and extrusive expanded polystyrene (penoplex) and a natural thermosyphon cooling system. Thus, the three models are: 0.45 cm thick foam glass (1); 0.45 cm thick penoplex (2), and 0.45 cm thick penoplex plus a thermosyphon (3). The thermosyphon seasonal cooling system consists of horizontal tubes with natural evaporation and condensation [*Dolgikh et al., 2008*], working as follows (Fig. 1). The tubes are filled with a cooling agent and placed in soil. Once the tubes become warmer than the condensation unit, the cooling agent evaporates taking the required heat from the soil. The vapor rises into the condenser, where it transforms back into liquid and then flows down by gravity into the tubes. The heat released during vapor condensation becomes transferred from soil to air, and the soil cools down. These cooling systems are operated only in winter, while in the warm season the soil between the building and the tubes is prevented from thawing with a thermal insulator.

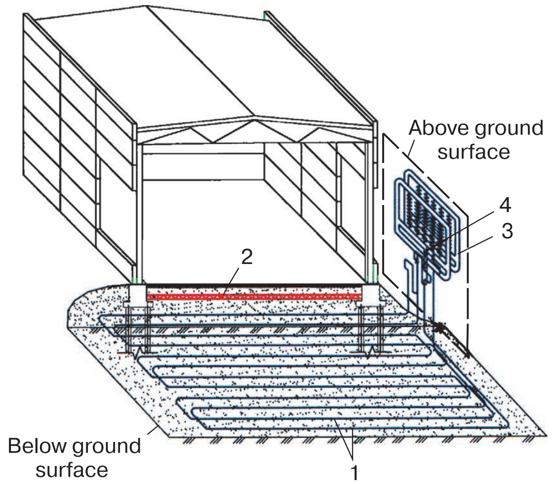

Fig. 1. A natural cooling system with horizontal tubes:

1 – cooling tubes; 2 – thermal insulation; 3 – condensation unit; 4 – circulation accelerator.

The thermosyphons regulate heat turnover naturally, without external powering, and are thus energy efficient and save the thermal energy of the soil-basement system.

PROBLEM FORMULATION

The model simulates a building, 46 m long and 24 m wide (Fig. 2) in the Cartesian coordinates, within a modeling domain of 100 m long, 100 m wide, and 10 m deep; the indoor temperature is 20 °C; the tubes of the cooling system lie 2.1 m below the building and are spaced at 0.5 m.

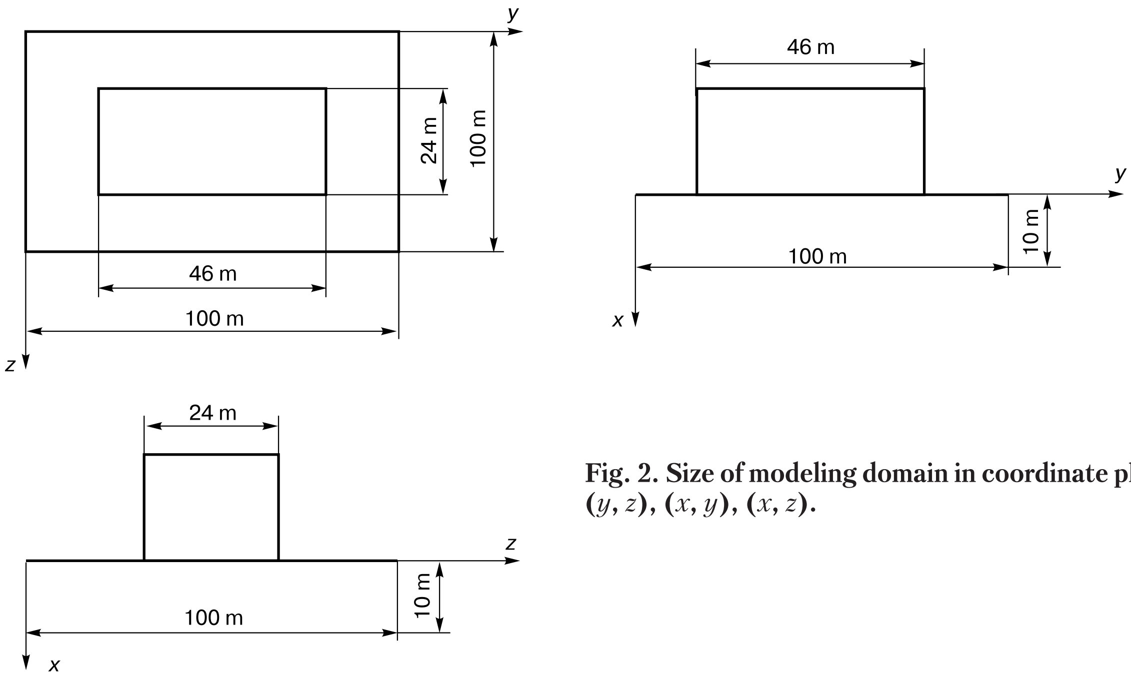

Fig. 2. Size of modeling domain in coordinate planes (y, z), (x, y), (x, z).

Heat and mass transfer in soil is estimated by the effective thermal conductivity method, with the thermal conductivity derived as [*Samarsky, 2003*]

$$\left[c+L\delta\left(t-t_p\right)\right]\frac{\partial t}{\partial \tau}=\lambda\left(\frac{\partial^2 t}{\partial x^2}+\frac{\partial^2 t}{\partial y^2}+\frac{\partial^2 t}{\partial z^2}\right), \qquad (1)$$

where c is the volumetric specific heat of soil; λ is the soil thermal conductivity; t is the temperature; t_p is the temperature of liquid-to-vapor phase transition; x, y, z are the Cartesian coordinates; τ is the time; $\delta(t - t_p)$ is the Dirac delta. L is given by

$$L = r(w - w_{\mathrm{ufw}})\gamma_{\mathrm{sk}},$$

where r is the specific heat of ice melting; w is the water content in soil; w_{ufw} is the content of unfrozen water in soil; γ_{sk} is the soil skeleton density.

The difference scheme corresponding to (1) is written as

$$\begin{aligned}&t(i,j,k,n+1)=t(i,j,k,n)+\\&+\frac{a(i,j,k)h_\tau}{h_x^2}\left[t(i+1,j,k,n)+t(i-1,j,k,n)-2t(i,j,k,n)\right]+\\&+\frac{a(i,j,k)h_\tau}{h_y^2}\left[t(i,j+1,k,n)+t(i,j-1,k,n)-2t(i,j,k,n)\right]+\\&+\frac{a(i,j,k)h_\tau}{h_z^2}\left[t(i,j,k+1,n)+t(i,j,k-1,n)-2t(i,j,k,n)\right], \qquad (2)\end{aligned}$$

where

$$a(i,j,k)=\begin{cases}a_{\mathrm{f}}, & t(i,j,k,n)<t_p-\Delta,\\ \dfrac{0.5(\lambda_{\mathrm{f}}+\lambda_{\mathrm{uf}})}{0.5(c_{\mathrm{f}}+c_{\mathrm{uf}})+L/2\Delta}, & t_p-\Delta\le t(i,j,k,n)\le t_p+\Delta,\\ a_{\mathrm{uf}}, & t(i,j,k,n)>t_p+\Delta.\end{cases}$$

There a_{uf} and a_{f} are the thermal diffusivities of unfrozen and frozen soil, respectively; λ_{uf} and λ_{f} are the thermal conductivities of unfrozen and frozen soil, respectively; c_{f}, c_{uf} are the volumetric heat capacities of unfrozen and frozen soil, respectively. In the effective heat capacity method [*Samarsky, 2003*], Δ refers to the phase transition temperature range: $t_p-\Delta\le t(i,j,k,n)\le t_p+\Delta$. When calculating $a(i, j, k)$, the Dirac delta in (1) is replaced by the function $f(t - t_p)$ [*Samarsky, 2003*]

$$f\left(t-t_p\right)=\begin{cases}0, & \left|t-t_p\right|>\Delta,\\ \dfrac{1}{2\Delta}, & \left|t-t_p\right|\le\Delta.\end{cases}$$

The space and time coordinates in the modeling domain, as well as the stability criterion of the explicit difference scheme, are

$$x_i = ih_x,\ 0 \le i \le i_{\max},$$

$$y_i = jh_y,\ 0 \le j \le j_{\max},$$

$$z_k = kh_z,\ 0 \le k \le k_{\max},$$

$$\tau_n = h_\tau n,\ 0 \le n \le n_{\max},$$

$$h_\tau \le \frac{1}{3a}\left(\frac{1}{h_x^2}+\frac{1}{h_y^2}+\frac{1}{h_z^2}\right)^{-1},$$

where $a = \max(a_{\mathrm{f}}, a_{\mathrm{uf}})$; $h_x = 0.1$ m, $h_y = 0.1$ m, $h_z = 1$ m are the grid spacing sizes along the coordinates x, y, and z, respectively; $h_\tau = 0.01$ day is the time stepsize; $i_{\max} = 101$, $j_{\max} = 1001$, $k_{\max} = 99$ are the maximum i, j, and k values that define the size of the modeling domain; $n_{\max}$ corresponds to the temperature sampling time.

The soil-air thermal interaction depends mostly on the radiation and convection heat fluxes. The radiation heat flux q_r on the soil (snow) surface is [*Pavlov, 1984*]

$$q_r = R(1-A) - \varepsilon\sigma T_s^4 (1-p),$$

where R is the incident solar radiation; A is the albedo; σ is the Stefan-Boltzmann constant; T_s is the surface temperature, in K; p is the share of the outgoing infrared heat radiated from the soil surface to the air and reflected back from the air to the soil; ε is the emissivity. The latter can be assumed to be about unity [*Pavlov, 1984*], while the global mean is $p = 0.84$ [*Trenberth et al., 2009*]. In our specific case its value is unknown, but we may use the global mean approximation because its contribution to the total heat flux is insignificant.

The convective heat flux q_c from the air to the soil (snow) is [*Foken, 2008*]:

$$q_c = \frac{\rho c_p (\alpha_0 \kappa)^2 v(z)\big(t(z) - t(0)\big)}{\big(\ln(z/z_0)\big)^2}, \qquad (3)$$

where ρ is the air density; c_p is the air specific heat; $\alpha_0 = 1.25$; $\kappa = 1.4$ is the Karman constant; $v(z)$ is the air (wind) speed at the height z above the surface; $t(z)$ is the temperature at the height z above the surface; $t(0)$ is the surface temperature.

The air temperature and the wind speed are commonly measured at about 2 m and 10 m above the surface, respectively. Finally, taking into account that [*Foken, 2008*]

$$v(z) = v(10)\frac{\ln(z/z_0)}{\ln(10/z_0)}, \qquad (4)$$

and substituting (4) into (3), we obtain the convective heat flux as

$$q_c = \frac{\rho c_p (\alpha_0 \kappa)^2 v(10)\big(t(z) - t(0)\big)}{\ln(z/z_0)\ln(10/z_0)},$$

where z is the height above the surface where air temperature is sampled at weather stations; z_0 is the terrain parameter proportional to the surface roughness. For the smooth snow surface, $z_0 = 0.001$ m and $A = 0.75$ [*Pavlov, 1984*], and for the soil surface the values are $z_0 = 0.02$ m and $A = 0.25$.

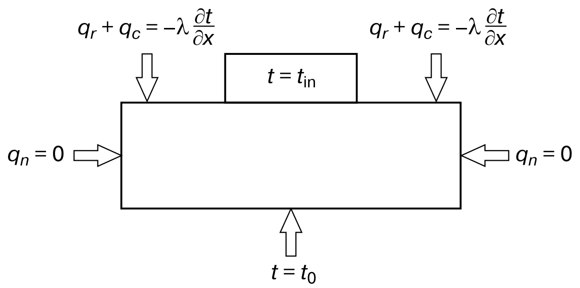

Fig. 3. Boundary conditions in modeling domain.

The incident solar radiation in different months is (borrowed from [*Pavlov, 1984*]):

Months	I	II	III	IV	V	VI
R, W/m^2	0	16	74	171	205	237
Months	VII	VIII	IX	X	XI	XII
R, W/m^2	224	129	60	22	3	0

The boundary conditions on the surface are

$$q_r + q_c = -\lambda \frac{\partial t}{\partial x},$$

where λ is the thermal conductivity of soil or snow, and x is the depth below the surface.

The boundary conditions within the modeling domain (Fig. 3) imply zero heat flux across the lateral surfaces ($q_n = 0$) and the first-kind boundary condition at the bottom. The coordinates are chosen such that the nodes fall on the tubes of the cooling system, which are assumed to be linear sources of cold. It is easy to calculate that the heat flux at a node crossed by a thermosyphon tube, with the numbers i, j, k along the coordinates x, y, z, respectively, is

$$U_{i,j,k} = \frac{\lambda_s h_x h_z}{h_y}\left(t_{i,j+1,k} + t_{i,j-1,k} - 2t_{\text{tube}}\right) + \\ + \frac{\lambda_s h_y h_z}{h_x}\left(t_{i+1,j,k} + t_{i-1,j,k} - 2t_{\text{tube}}\right),$$

where λ_s is the soil thermal conductivity; t_{tube} is the tube temperature.

The heat flux between the evaporator and the air is defined by the boundary condition

$$\sum_{i,j,k\in M} U_{i,j,k} = S_{\text{con}} N_{\text{con}} \eta_{\text{eff}} (t_c - t_a)\alpha,$$

where M is the set of nodes crossed by the tubes; S_{con} is the surface area of a single condenser; N_{con} is the number of condensers; η_{eff} is the fin efficiency; t_c is the temperature of the condenser; t_a is the air temperature; α is the heat transfer coefficient of the condenser.

To estimate the condenser temperature [*Anikin et al., 2011*], one has to know the temperature of the evaporator, which in its turn equals the soil temperature at the contact with the tube:

$$t_c = t_{\text{tube}} - \frac{0.5\rho_{\text{ca}} g H}{dp_{\text{sat}}/dt},$$

where ρ_{ca} is the cooling agent density; g is the acceleration due to gravity; H is the height of the condenser above the evaporator; dp_{sat}/dt is the temperature derivative of the saturated vapor pressure. The calculated temperatures show good fit to the measured values [*Dolgikh et al., 2013*]. The heat flux is modeled presuming that the weather data are probabilistic. The probabilistic methods have been applied to foundation design since the 1980s [*Khrustalev and Pustovoit, 1988*].

STOCHASTIC ANALYSIS

The long-term thermal behavior of soil is usually predicted from monthly mean air temperature, wind speed, and snow thickness values which repeat from year to year, but this approach is restricted to single-scenario prediction. Alternatively, probabilistic prediction using stochastic analysis [*Anikin et al., 2013*] can account for the whole diversity of possible scenarios. The method uses synthetic air temperature, wind speed, and snow thickness values generated as random numbers based on their probability distributions according to weather station records. The modeling gives multiple predicted 3D temperature fields beneath a structure, each corresponding to one possible scenario, which jointly provide a complete picture of the future soil behavior.

For instance, the probability distributions of air temperatures recorded at the Igarka weather station turned out to fit the normal law

$$dw(t) = \frac{\exp\left[-(t-\bar{t})^2/2\sigma^2\right]dt}{\sqrt{2\pi}\sigma}$$

(where t is the temperature; $\bar{t}$ is the mathematical expectation; σ is the rms error), while the wind speed showed a gamma distribution:

$$dw(v) = \frac{\lambda^{\alpha}}{\Gamma(\alpha)} v^{\alpha-1} e^{-\lambda v} dv,$$

where v is the wind speed; $\Gamma(\alpha)$ is the gamma function; and α and λ are related with the average wind speed $\bar{v}$ and dispersion (variance) D as

$$\bar{v} = \alpha/\lambda, \quad D = \alpha/\lambda^2.$$

The distributions of the synthetic weather parameters for June and January obtained using the *MathCAD-14* random number generator (Fig. 4) agree well with those of the Igarka station. Similar synthetic curves were plotted for other months as well

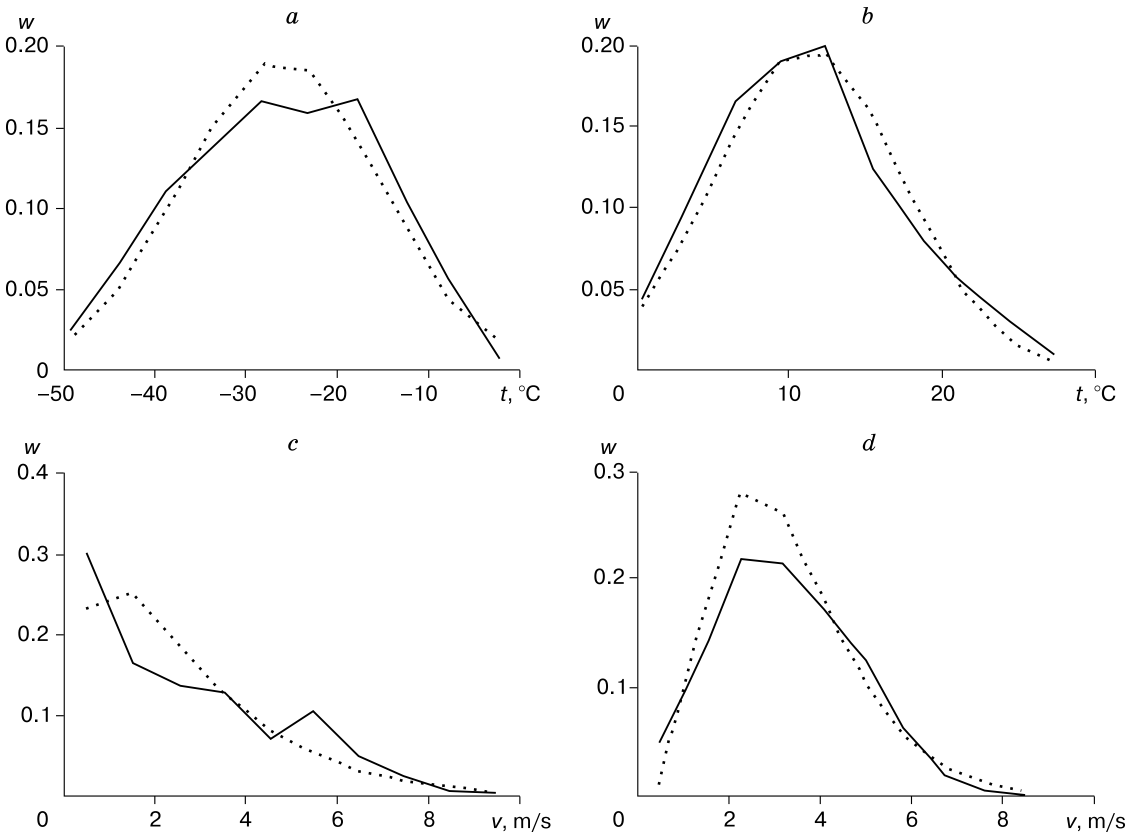

Fig. 4. Temperature and wind speed patterns in June and January according to Igarka weather station records in 2007 through 2012 (solid lines), compared with the respective synthetic patterns obtained by *MathCAD-14* random number generators.

a: solid line shows January temperatures, dashed line is normal distribution with σ = 10.768 °C, $\bar{t}$ = –26.225 °C, obtained with the random number generator; *b*: solid line shows June temperatures, dashed line is normal distribution with σ = 5.99 °C, $\bar{t}$ = 11.22 °C, obtained with the random number generator; *c*: solid line shows January wind speed, dashed line is gamma distribution with α = 1.606, λ = 0.588, obtained with the random number generator; *d*: solid line shows June wind speed, dashed line is gamma distribution with α = 4.536, λ = 1.392, obtained with the random number generator.

Table 1. **Monthly patterns of air temperature, wind speed, and snow thickness**

Parameter	Janu.	Febr.	March	Apr.	May	June	July	Aug.	Sent.	Oct.	Nov.	Dec.
$\bar{t}$, °C	–26.20	–27.0	–17.30	–8.12	–0.66	11.20	15.80	11.30	6.60	–4.20	–19.10	–24.40
σ, °C	10.80	9.88	10.20	9.24	6.34	5.99	5.18	4.41	4.86	7.29	11.13	11.40
α	1.61	1.54	1.91	2.40	3.66	4.54	2.15	2.68	2.77	2.84	1.58	2.18
λ, c/m	0.59	0.60	0.64	0.75	1.06	1.39	0.91	0.94	0.88	0.87	0.59	0.70
$\bar{h}$, m	0.70	0.79	0.86	0.79	0.48	0	0	0	0	0.12	0.35	0.53
σ_h, m	0.21	0.19	0.19	0.20	0.22	0	0	0	0	0.10	0.13	0.17

(not shown here for the limited paper size) and all showed quite a good fit to the observations (Table 1).

The statistical sample of snow thickness records at the Igarke station is limited and insufficient for obtaining a smooth distribution; for this reason, the parameter was modeled using the normal distribution with the mathematical expectation $\bar{h}$ and the sigma error σ_h given by

$$\bar{h} = \sum_i \frac{h_i}{N}, \quad \sigma_h = \sqrt{\sum_i \frac{(h_i - \bar{h})^2}{N}},$$

where h_i is the specific snow thickness value in the sample for a given month and N is the size of the data sample for the respective month. Summation is over the whole sample. The values of $\bar{h}$ and σ_h for each month are given in Table 1, and both are assumed to be zero ($\bar{h}$ = 0, σ_h = 0) in the warm season (from June through September).

THREE OPTIONS FOR SOIL INSULATION, COMPARED

The modeling was performed on an *NCS-30T* supercomputer at the Siberian Supercomputing Center. Monte-Carlo simulation put out 48 scenarios of soil behavior, with the solar radiation R as quoted above and air temperatures obtained by the *MathCAD-14*

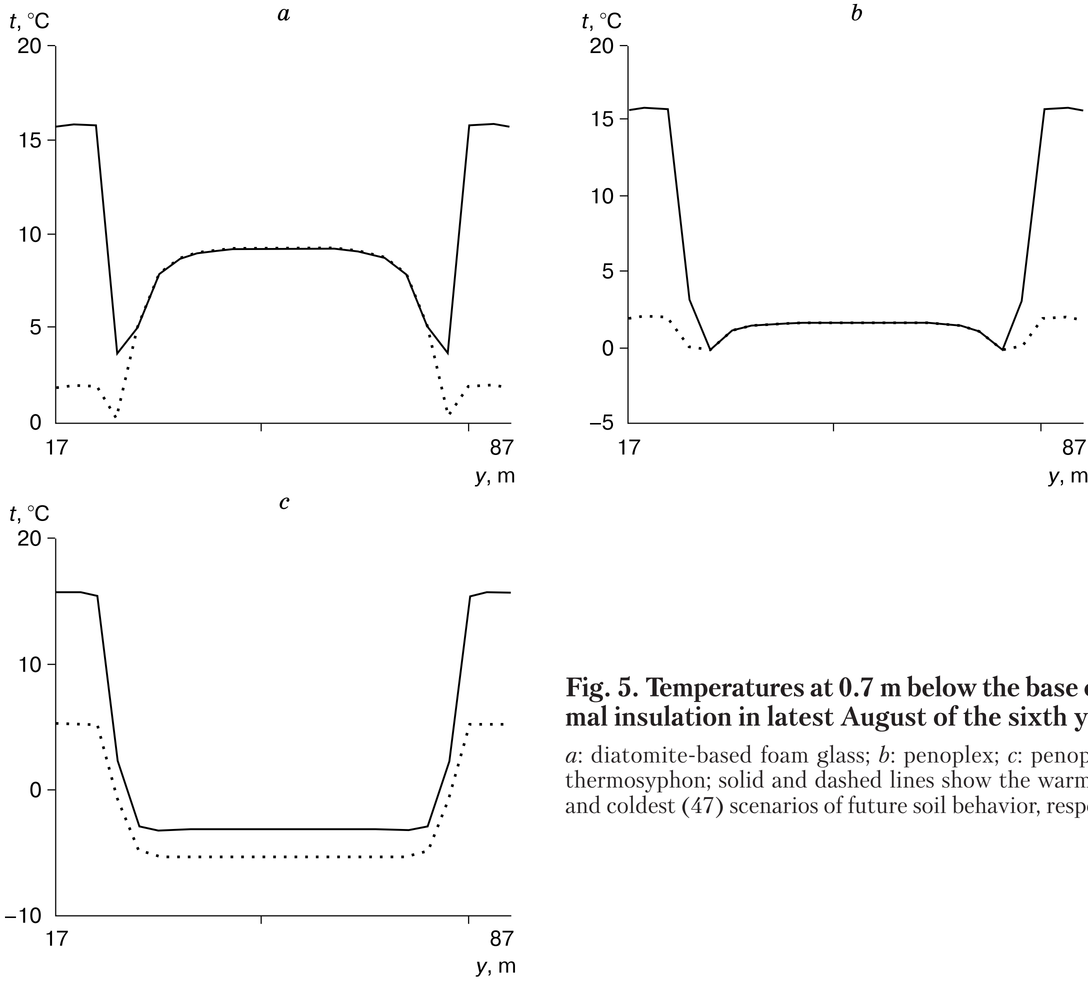

Fig. 5. Temperatures at 0.7 m below the base of thermal insulation in latest August of the sixth year.

a: diatomite-based foam glass; *b*: penoplex; *c*: penoplex plus thermosyphon; solid and dashed lines show the warmest (27) and coldest (47) scenarios of future soil behavior, respectively.

random number generator. The calculations were for six arbitrary years, beginning with September (a month of an arbitrary year), assuming that $\lambda_f = 2$ W/(m·K), $\lambda_{uf} = 1.4$ W/(m·K), $w = 0.25$, $c_f = 2390$ kJ/(m^3·K), $c_{uf} = 3010$ kJ/(m^3·K), $\gamma_{sk} = 1620$ kg/m^3. The temperature curves in Fig. 5 are for 0.7 m below the base of the thermal insulator plate, with the highest and lowest mean temperatures on the line in the latest August of the sixth modeling year. In the absence of a thermosyphon, the soil temperature beneath the building is fully controlled by the heat flux from the latter and is almost independent of weather (Fig. 5).

The models in Fig. 6 represent the temperature fields beneath the building for each case, in the latest August of the sixth year. In the case of thermal insulation alone, the thaw depths of soil are 6 m and 2 m for diatomite-based foam glass (Fig. 6, *a*) and penoplex (Fig. 6, *b*), respectively.

The foam glass is a porous inorganic material obtained by foaming at 750–850 °C of a siliceous composite based on diatomaceous earth, which is a sedimentary rock found everywhere worldwide. For instance, the resources of diatomite exposed in the Yamal Peninsula count hundreds of billions of cubic meters. Thermal insulation of foundations beneath engineering structures and buildings using diatomite-based foam glass, with its thermal conductivity 0.10–0.15 W/(m·K), may be advantageous because the material (i) can bear compressive loads up to 50 kgs/cm^2; (ii) has closed porosity and does not absorb moisture when lying at the foundation thus

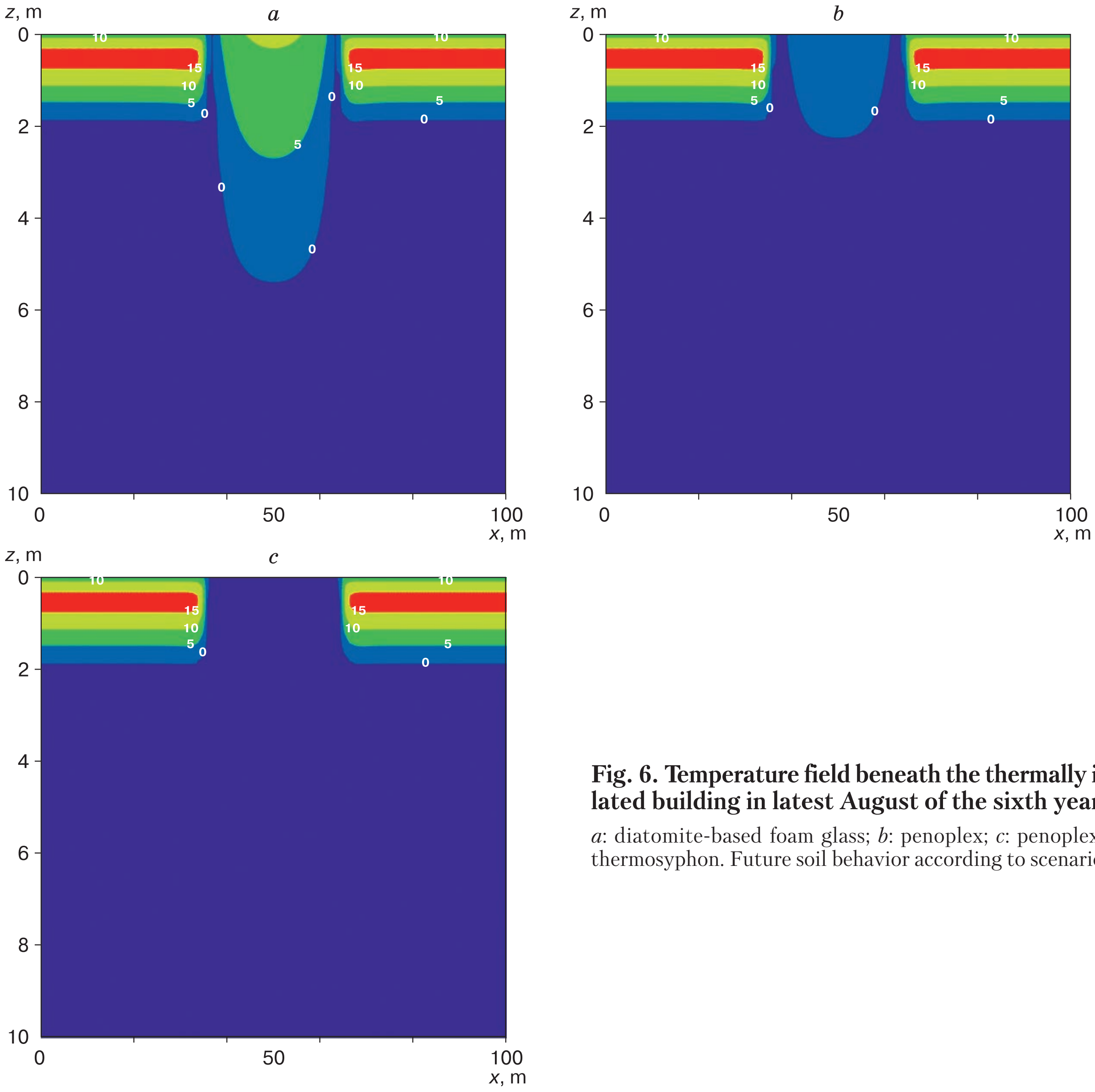

Fig. 6. Temperature field beneath the thermally insulated building in latest August of the sixth year.

a: diatomite-based foam glass; *b*: penoplex; *c*: penoplex plus thermosyphon. Future soil behavior according to scenario 27.

keeping its insulation property; (iii) is inflammable till 550 °C (unlike the conventional insulators) and highly durable. Diatomite foam glass may have diverse uses as various products: plates, shells, wall blocks, rounded granules, etc.

However, thermal insulation alone makes no sense as it cannot fully protect the permafrost, and the soil will thaw sooner or later (Fig. 6, *a*, *b*) unless thermosyphons are used (Fig. 6, *c*). The curves for 0.7 m below the insulation base (Fig. 5) show that in the absence of thermosyphons, the soil temperature depends only on heat flux from the building and on thermal insulation but is independent of weather (Fig. 5, *a*, *b*); however, the soil temperature becomes sensitive to air temperature variations if the cooling systems are on (Fig. 5, *c*) because they exchange heat with air.

The heat loss through the building sides can be estimated as follows. The total annual heat flux through the side walls is

$$Q = \lambda_{\text{wall}} (t_{\text{in}} - t_{\text{a}}) \frac{S}{h},$$

where λ_{wall} is the thermal conductivity of the walls; t_{in} is the indoor temperature; t_{a} is the air temperature; S is the surface area of the walls; h is the wall thickness. Assuming that the building is 10 m high and the surface area of windows is 20 % of the total area of the side walls, the heat loss through walls of different materials will be: Q = 9.6 kW at λ_{wall} = 0.15 W/(m·K) for diatomite-based foam glass; Q = 44.8 kW at λ_{wall} = 0.7 W/(m·K) for brick walls.

This is mean annual heat flux through the side walls averaged over all future scenarios because the mean annual value, averaged over all versions, is ($t_{\text{in}} - t_{\text{a}}$) = 28.56 K, according to the numerical experiment. Thus, diatomite-based foam glass can provide multi-fold heat saving.

CONCLUSIONS

The reported probabilistic prediction shows that the thermal field beneath the building does not depend on air temperature, wind speed, and snow thickness in the absence of seasonal cooling systems (Fig. 5, *a*, *b*). The lateral heat loss is insignificant and rough estimates of heat flux at the soil-air boundary are sufficient without taking into account the weather effects. The inference that the soil-air heat exchange does not cause much influence on the thermal field beneath large buildings may be useful in foundation design. Without thermosyphon cooling, thaw depth can reach 6 m for six years (Fig. 6, *a*) but soil remains always frozen when cooled with the seasonal systems (Fig. 6, *c*). Therefore, thermosyphons are indispensable in the absence of ventilated cellars. Currently many engineering structures, such as oil or gas pipelines, are built in permafrost without additional cooling presuming that thermal insulation alone can prevent soil from thawing. This strategy however has deplorable consequences: gas lines sink or emerge, oil lines break down, and buildings subside in creeping soil. Meanwhile, the use of thermosyphons along with good thermal insulation can keep the soil frozen even in the end of summer (Fig. 6, *c*).

The natural-circulation thermosyphons which consume no electric energy can provide more energy efficient operation of structures built on permafrost than the refrigerator systems.

The study has been supported by grant 14-17-000131 from the Russian Science Foundation.

References

Anikin, G.V., Plotnikov, S.N., Spasennikova, K.A., 2011. Computer simulation of heat-mass exchange in the systems of horizontal ground cooling. Kriosfera Zemli XV (1), 33–39.

Anikin, G.V., Plotnikov, S.N., Vakulin, A.A., Spasennikova, K.A., 2013. Probabilistic prediction of soil behavior under structures built on permafrost. Bull. Tyumen University, No. 7, 46–53.

Dolgikh, G.M., Okunev, S.N., Anikin, G.V., Spasennikova, K.A., 2013. Numerical calculation of unsteady temperature fields in the system "oil tank–seasonal cooling system". Kriosfera Zemli XVII (3), 70–75.

Dolgikh, G.M., Okunev, S.N., Podenko, L.S., Feklistov, V.N., 2008. Safety, efficiency, and management of systems for thermal stabilization of frozen soil under engineering and civil structures, in: Permafrost Resources of High-latitude and Highland Regions. State and Prospects of Permafrost Engineering, Proc. Intern. Conf., Tyumen, FSA R&D LLC, pp. 34–39.

Foken, T., 2008. Micrometeorology. Springer, Berlin, etc., 306 pp.

Khrustalev, L.N., Pustovoit, G.P., 1988. Probabilistic Foundation Design in Permafrost. Nauka, Moscow, 249 pp. (in Russian)

Pavlov, A.V., 1984. Energy Exchange in the Terrestrial Landscapes. Nauka, Novosibirsk, 256 pp. (in Russian)

Samarsky, A.A., 2003. Heat Transfer Simulation. Editorial URSS, Moscow, 784 pp. (in Russian)

Trenberth, K.E., Fasullo, J.T., Kienl, J., 2009. Earth's global energy budget. Amer. Meteorol. Soc., March, 311–323.

Received March 25, 2014